RESEARCH ARTICLE

Figures and figure supplements

Structure-guided microbial targeting of antistaphylococcal prodrugs

Justin J Miller *et al*

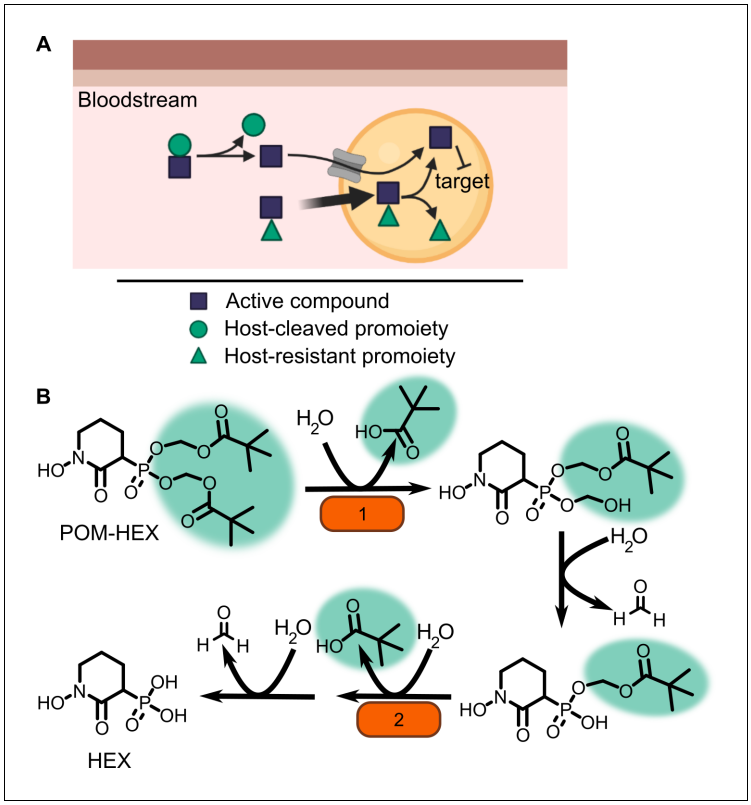

Figure 1. Prodrug activation model (A) and proposed enzymatic mechanism. (B) Carboxy ester promoieties highlighted in green.

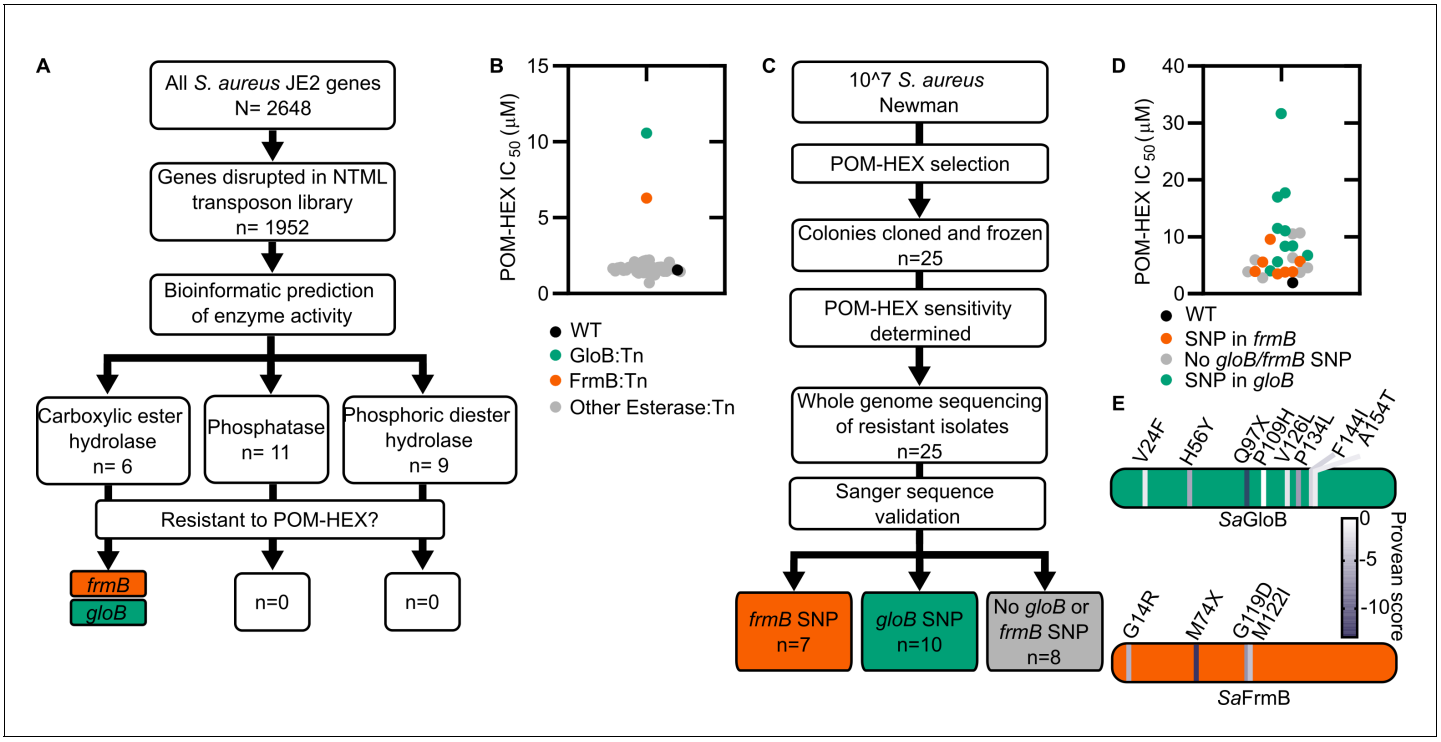

Figure 2. Forward and reverse genetics approaches identify FrmB and GloB as candidate POM-prodrug hydrolases in *S. aureus*. (**A**) Reverse genetics identification of candidate prodrug activating enzymes. (**B**) POM-HEX susceptibility of identified candidate resistance genes from (**A**) as determined by IC_{50}. Exact values and error reported in ***Figure 2—source data 1***. (**C**) Forward genetic screen approach, all mutations listed in ***Figure 2—source data 2***. (**D**) POM-HEX susceptibility of POM-HEX-resistant *S. aureus*. (**E**) Nonsynonymous point mutations identified by whole-genome sequencing in *frmB* and *gloB*. In all experiments, GloB is colored green and FrmB orange. Displayed are the means of three independent biological experiments.

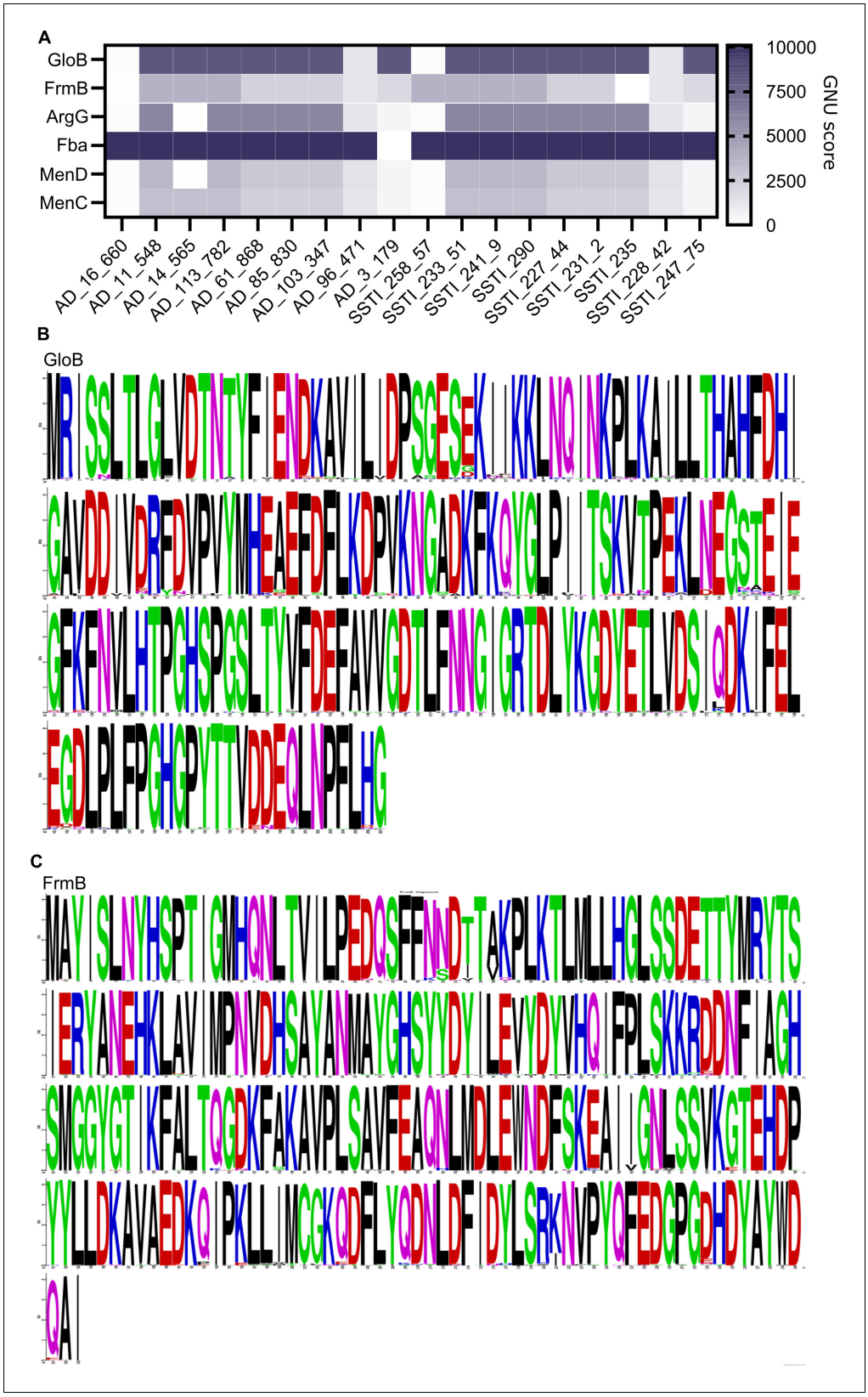

Figure 2—figure supplement 1. Conservation of FrmB and GloB within *S. aureus*. (**A**) WhatsGNU analysis of GloB and FrmB. Control proteins: ArgG, argininosuccinate synthase; Fba, fructose-bisphosphate aldolase; MenD, 2-succinyl-5-enolpyruvyl-6-hydroxy-3-cyclohexene-1carboxylate synthase; and MenC, o-succinylbenzoate synthase.

Figure 2—figure supplement 1 continued on next page

Figure 2—figure supplement 1 continued

GNU stands for gene novelty unit and is a count of how many protein sequences in the database have an exact match to the queried sequence, with higher counts indicating sequence conservation. Strains across the x-axis are representative strains from the 18 *s. aureus* colony complexes which were used to query the *S. aureus* database. (**B, C**) MAFFT alignment of GloB (**B**) and FrmB (**C**) protein sequences across the *S. aureus* sequence database.

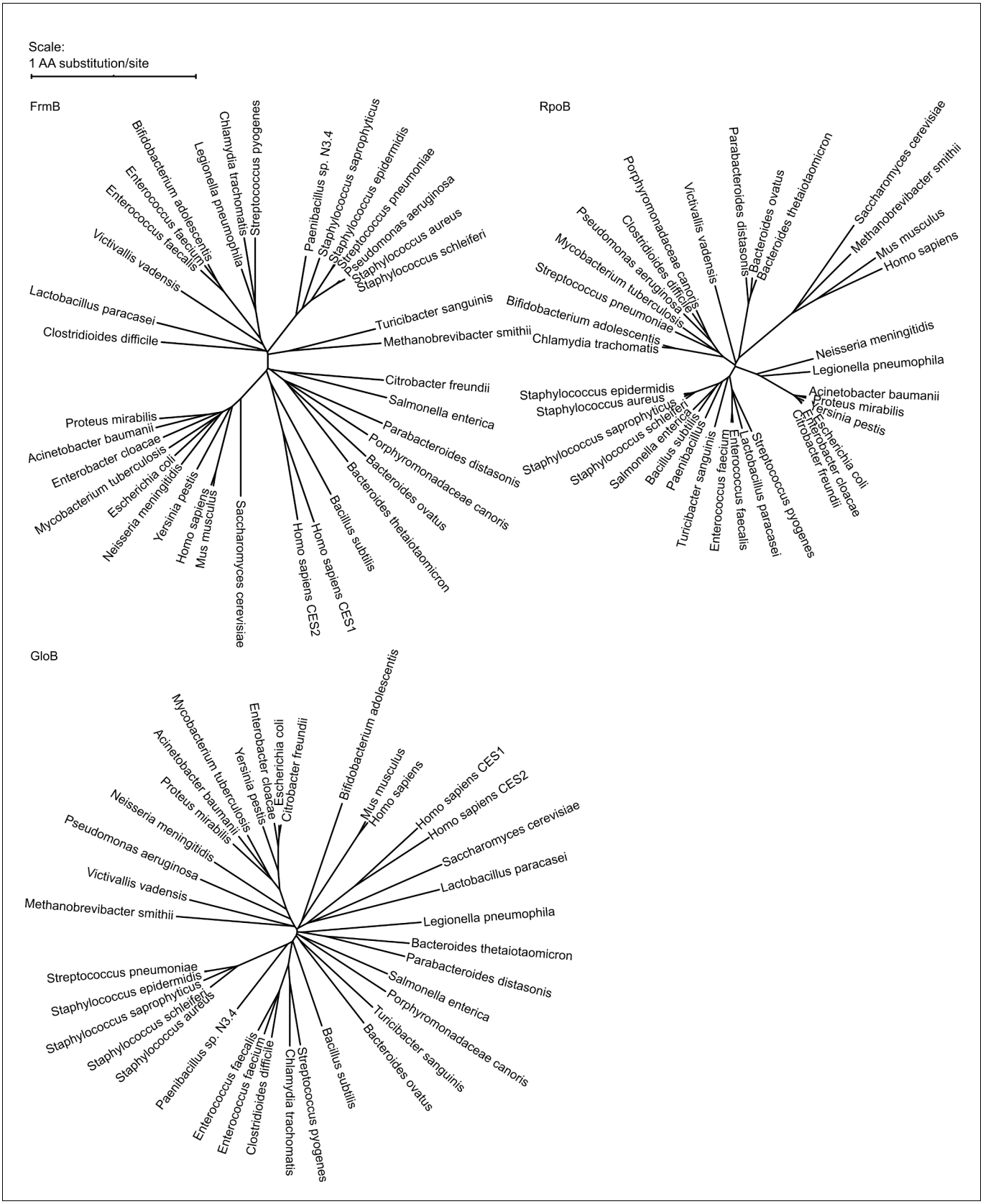
Scale:
1 AA substitution/site
FrmB
Streptococcus pyogenes
Chlamydia trachomatis
Legionella pneumophila
Bifidobacterium adolescentis
Enterococcus faecium
Enterococcus faecalis
Victivallis vadensis
Lactobacillus paracasei
Clostridioides difficile
Paenibacillus sp. N3.4
Staphylococcus saprophyticus
Staphylococcus epidermidis
Streptococcus pneumoniae
Pseudomonas aeruginosa
Staphylococcus aureus
Staphylococcus schleiferi
Turicibacter sanguinis
Methanobrevibacter smithii
Citrobacter freundii
Salmonella enterica
Parabacteroides distasonis
Porphyromonadaceae canoris
Bacteroides ovatus
Bacteroides thetaiotaomicron
Bacillus subtilis
Homo sapiens CES2
Homo sapiens CES1
Saccharomyces cerevisiae
Proteus mirabilis
Acinetobacter baumanii
Enterobacter cloacae
Mycobacterium tuberculosis
Escherichia coli
Neisseria meningitidis
Yersinia pestis
Homo sapiens
Mus musculus
RpoB
Porphyromonadaceae canoris
Clostridioides difficile
Pseudomonas aeruginosa
Mycobacterium tuberculosis
Streptococcus pneumoniae
Bifidobacterium adolescentis
Chlamydia trachomatis
Victivallis vadensis
Parabacteroides distasonis
Bacteroides ovatus
Bacteroides thetaiotaomicron
Saccharomyces cerevisiae
Methanobrevibacter smithii
Mus musculus
Homo sapiens
Neisseria meningitidis
Legionella pneumophila
Acinetobacter baumanii
Proteus mirabilis
Yersinia pestis
Escherichia coli
Enterobacter cloacae
Citrobacter freundii
Staphylococcus epidermidis
Staphylococcus aureus
Staphylococcus saprophyticus
Staphylococcus schleiferi
Salmonella enterica
Bacillus subtilis
Paenibacillus
Turicibacter sanguinis
Enterococcus faecium
Enterococcus faecalis
Lactobacillus paracasei
Streptococcus pyogenes
GloB
Bifidobacterium adolescentis
Mus musculus
Homo sapiens
Homo sapiens CES1
Homo sapiens CES2
Saccharomyces cerevisiae
Lactobacillus paracasei
Legionella pneumophila
Bacteroides thetaiotaomicron
Parabacteroides distasonis
Salmonella enterica
Porphyromonadaceae canoris
Turicibacter sanguinis
Bacteroides ovatus
Bacillus subtilis
Streptococcus pyogenes
Chlamydia trachomatis
Clostridioides difficile
Enterococcus faecium
Enterococcus faecalis
Paenibacillus sp. N3.4
Staphylococcus aureus
Staphylococcus schleiferi
Staphylococcus saprophyticus
Staphylococcus epidermidis
Streptococcus pneumoniae
Methanobrevibacter smithii
Victivallis vadensis
Pseudomonas aeruginosa
Neisseria meningitidis
Proteus mirabilis
Acinetobacter baumanii
Yersinia pestis
Enterobacter cloacae
Escherichia coli
Citrobacter freundii
Mycobacterium tuberculosis

Figure 2—figure supplement 2. Phylogenetic tree of FrmB and GloB. Sequences of GloB, FrmB, and RpoB (encoding the beta subunit of RNA polymerase, included for comparison) were retrieved from NCBI using BlastP against each organism. Sequence alignment performed using MUSCLE and alignment visualized using the interactive Tree of Life (iTOL).

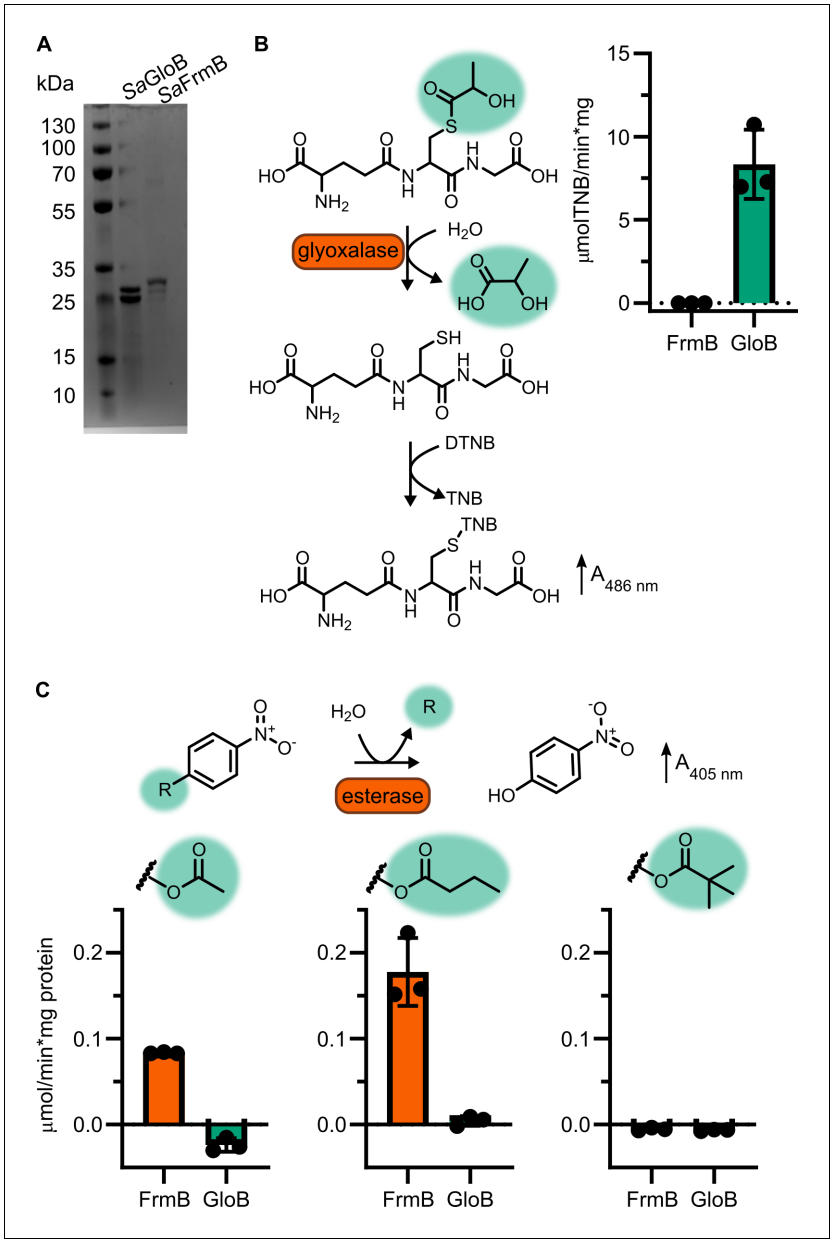

Figure 2—figure supplement 3. Enzymatic characterization of GloB and FrmB. (**A**) SDS–PAGE gel of GloB and FrmB protein preparations. Expected molecular weights are 23.3 kDa and 29.5 kDa, respectively. (**B**) Glyoxalase II activity assay, enzymatic conversion of S-lactoylglutathione releases free glutathione and reacts with DTNB resulting in increased absorbance at 412 nm. (**C**) 4-Nitrophenyl activation results in increased absorbance at 405 nm. Left to right, activity when supplied 4-nitrophenyl acetate, 4-nitrophenyl butyrate, and 4-nitrophenyl trimethyl acetate. Displayed in points is the mean of two technical replicates for individual experiments, bars indicate mean ± SD of three independent biological experiments performed in technical duplicate.

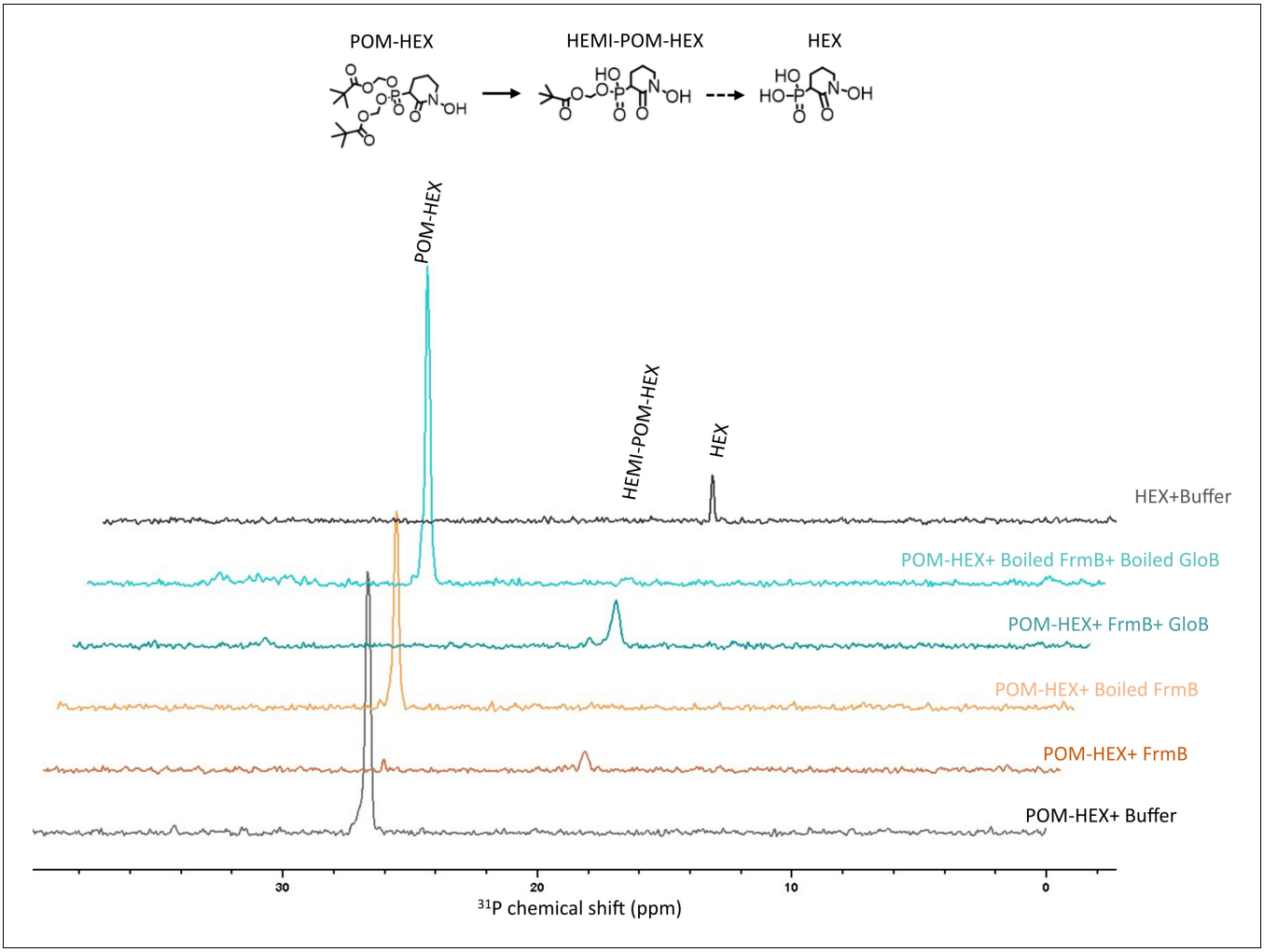

Figure 2—figure supplement 4. NMR characterization of POM-HEX activation by GloB and FrmB. Two-dimensional (2D) ^{1}H-^{31}P HSQC NMR spectra of products following incubation of FrmB, GloB, catalytically inactive (boiled) GloB and FrmB, or buffer alone. Also included are the ^{1}H-^{31}P HSQC NMR spectra of POM-HEX and HEX. Displayed are representative traces of three independent experiments. HEMI-POM HEX peak inferred by predicted shift.

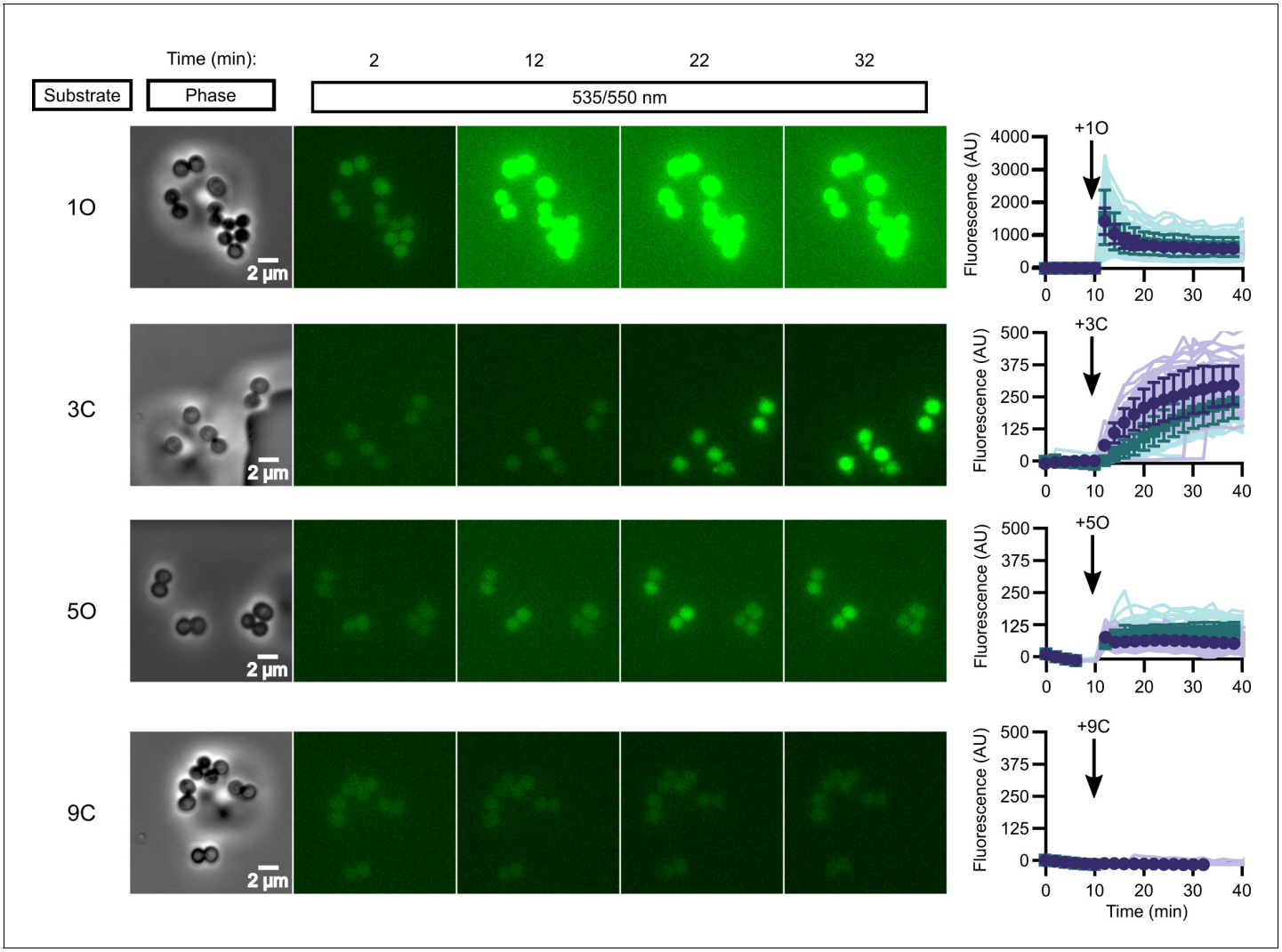

Figure 3. In vivo activation rates depend on ester promoiety selection. Time series of activation of various fluorogenic substrates (***Figure 3—figure supplement 1***). Substrates were added into the microfluidics chamber at t = 10 minutes. On the right, quantification of individual cell or cell cluster fluorescence per area. Faint traces are individual cells and darker traces represent the mean of a given experiment. Each experiment was performed in biological duplicate, and each experiment is displayed in a different color (purple or green). Full movies viewable as ***Videos 1–4***. Error bars denote SD.

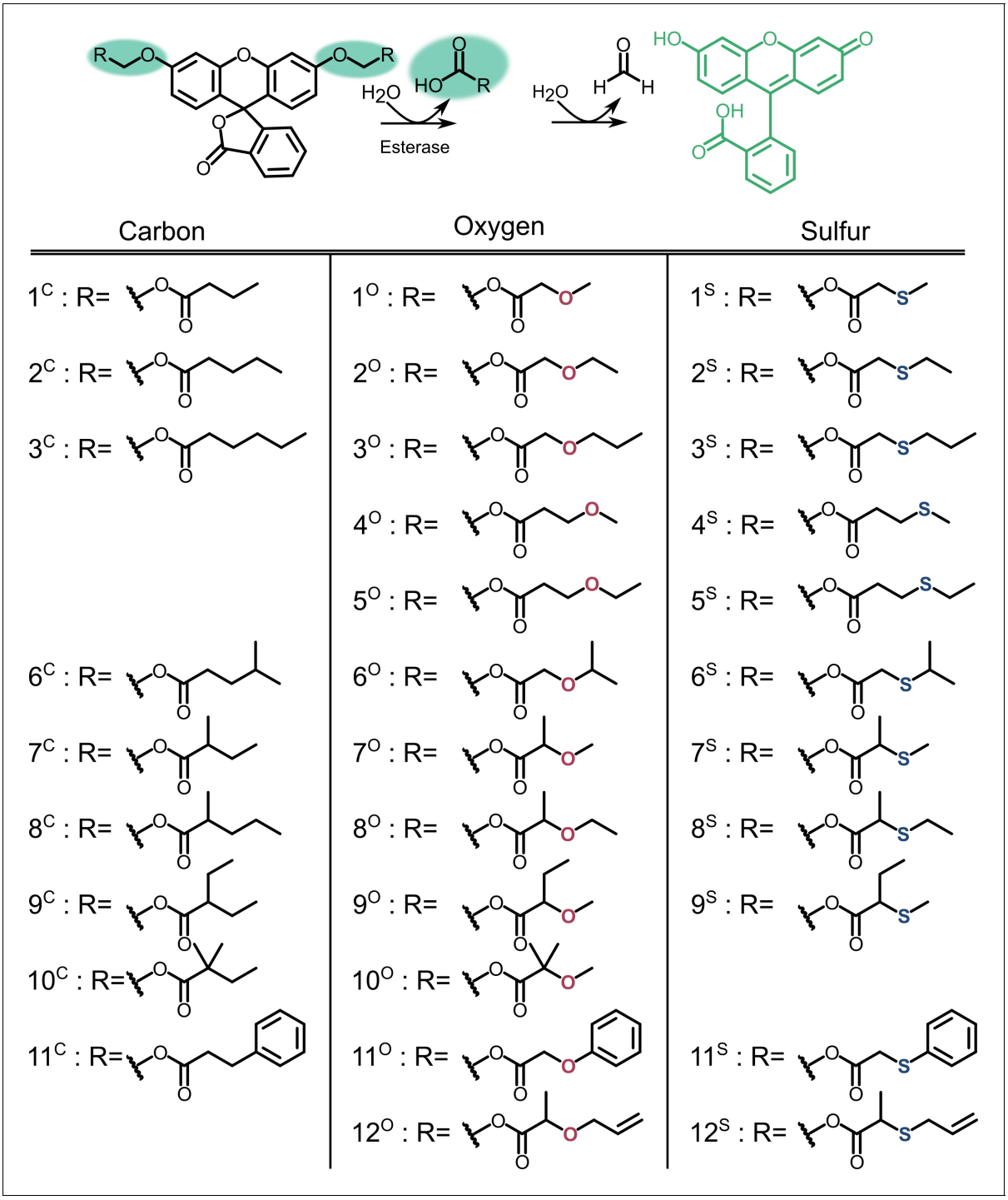

Figure 3—figure supplement 1. Profluorescent substrate library. Activation of substrates via esterase action results in fluorescence.

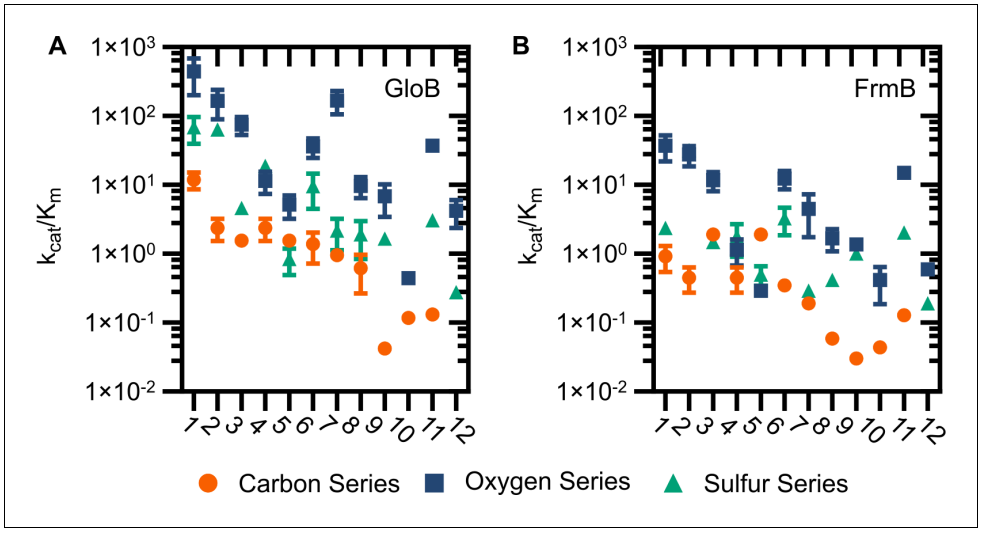

Figure 3—figure supplement 2. Catalytic efficiency of GloB (**A**) and FrmB (**B**). Numbers correspond to the structures displayed in Figure S5, compounds in the carbon series denoted in orange, oxygen series in blue, and sulfur series in green.

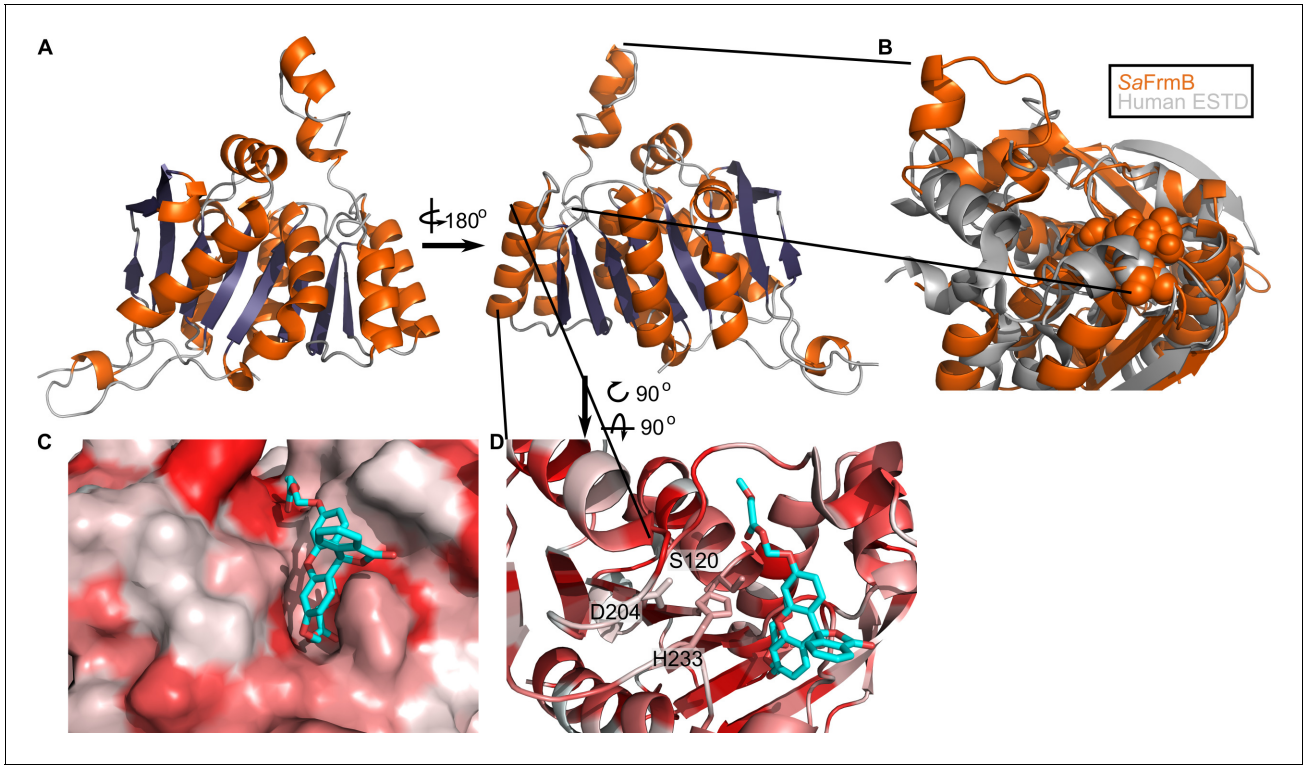

Figure 4. Three-dimensional structure of FrmB. (**A**) Overall fold, a-helices colored in orange and β-strands colored in purple. (**B**) Comparison between SaFrmB (orange) and its closest human ortholog, ESTD (gray). Active site residues denoted in orange spheres. (**C**, **D**) Docking of substrate 1O (sticks) in the active site of FrmB. surface view, red indicates highly hydrophobic and white hydrophilic residues. Surface view (**C**) or stick view with catalytic triad (**D**).

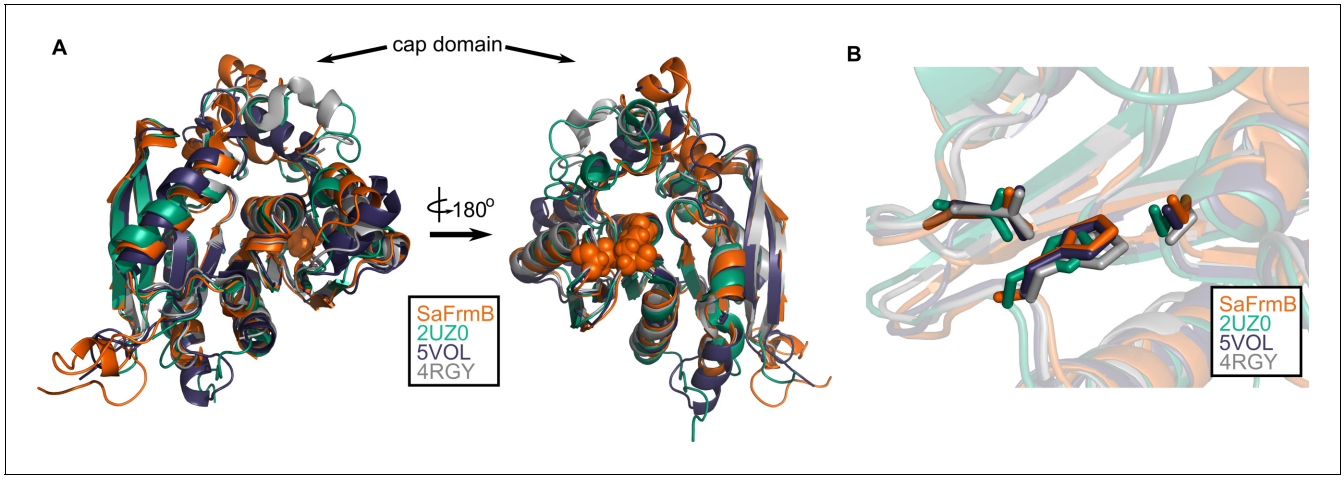

Figure 4—figure supplement 1. Structural conservation of FrmB. (**A**) Overall structural alignment of FrmB (orange) with *S. pneumonia* EstA (PDB:2UZ0), *B. intestinalis* ferulic acid esterase (PDB:5VOL), and deep sea bacteria Est12 (PDB4RGY). (**B**) Conservation of the serine hydrolase catalytic triad in FrmB and related proteins.

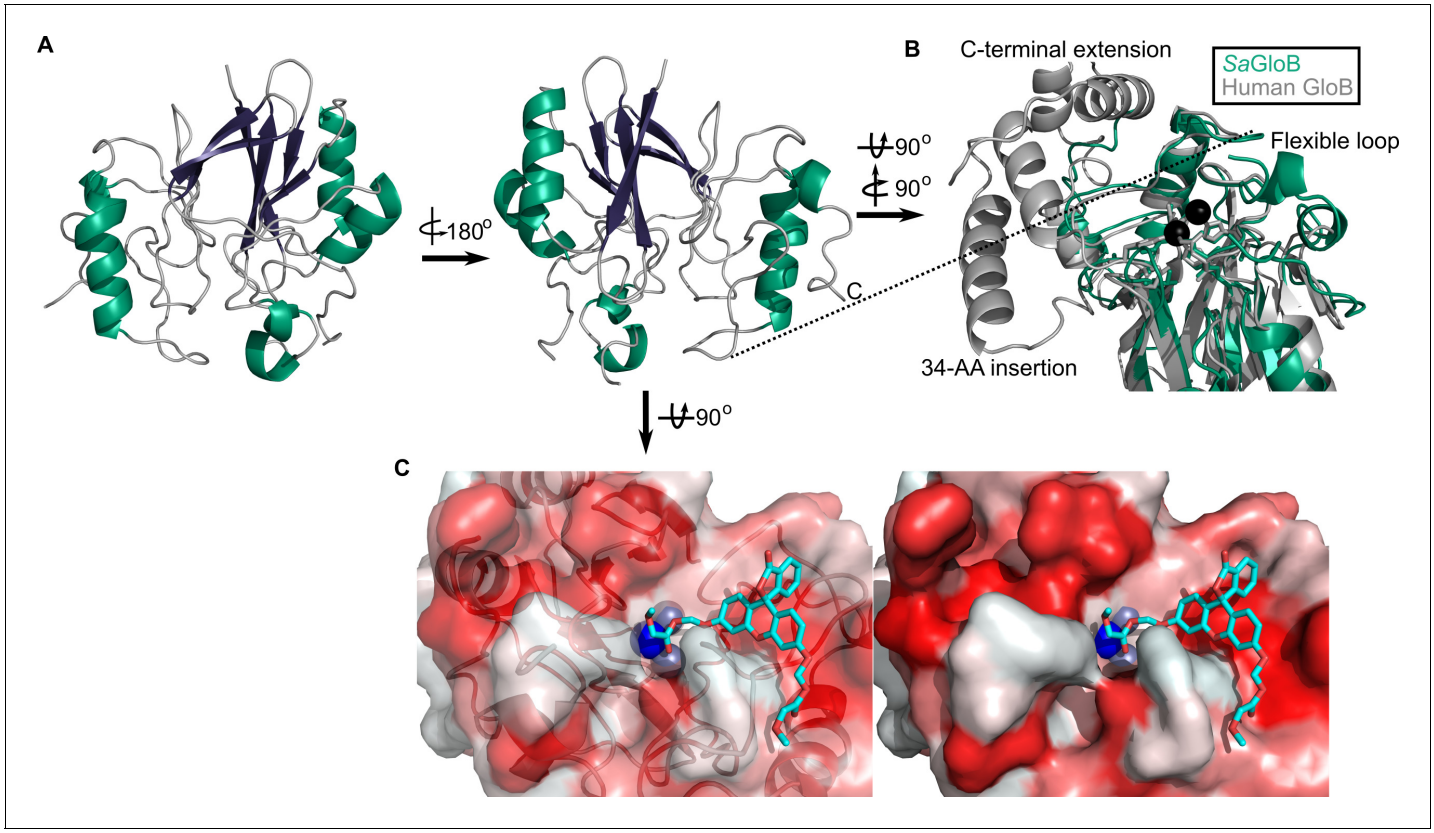

Figure 5. Three-dimensional structure of GloB. (**A**) Overall fold, a-alpha helices colored in green and β-strands colored in purple. (**B**) Comparison of SaGloB (green) and human GloB (gray). (**C**) Docking of the substrate 1O (sticks) in the active site of GloB. Left, partial cartoon view; right, surface view. White represents hydrophilic residues, whereas red represents hydrophobic residues. Zn ions indicated as silver spheres; water indicated as blue sphere.

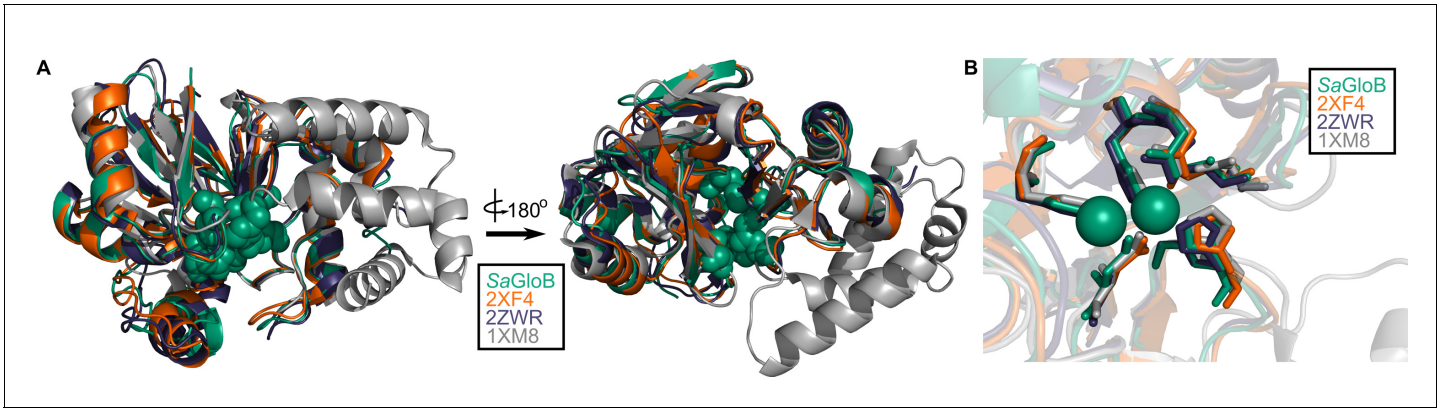

Figure 5—figure supplement 1. Structural conservation of GloB. (**A**) Overall structural alignment of GloB (green) with *S. enterica* YcbI (PDB:2XF4), *T. thermophilus* TTHA1623 (PDB:2ZWR), and *A. thaliana* glyoxalase II (PDB:1XM8). Zinc coordinating residues are colored in green spheres. (**B**) Positioning of the zinc coordinating residues (green spheres).

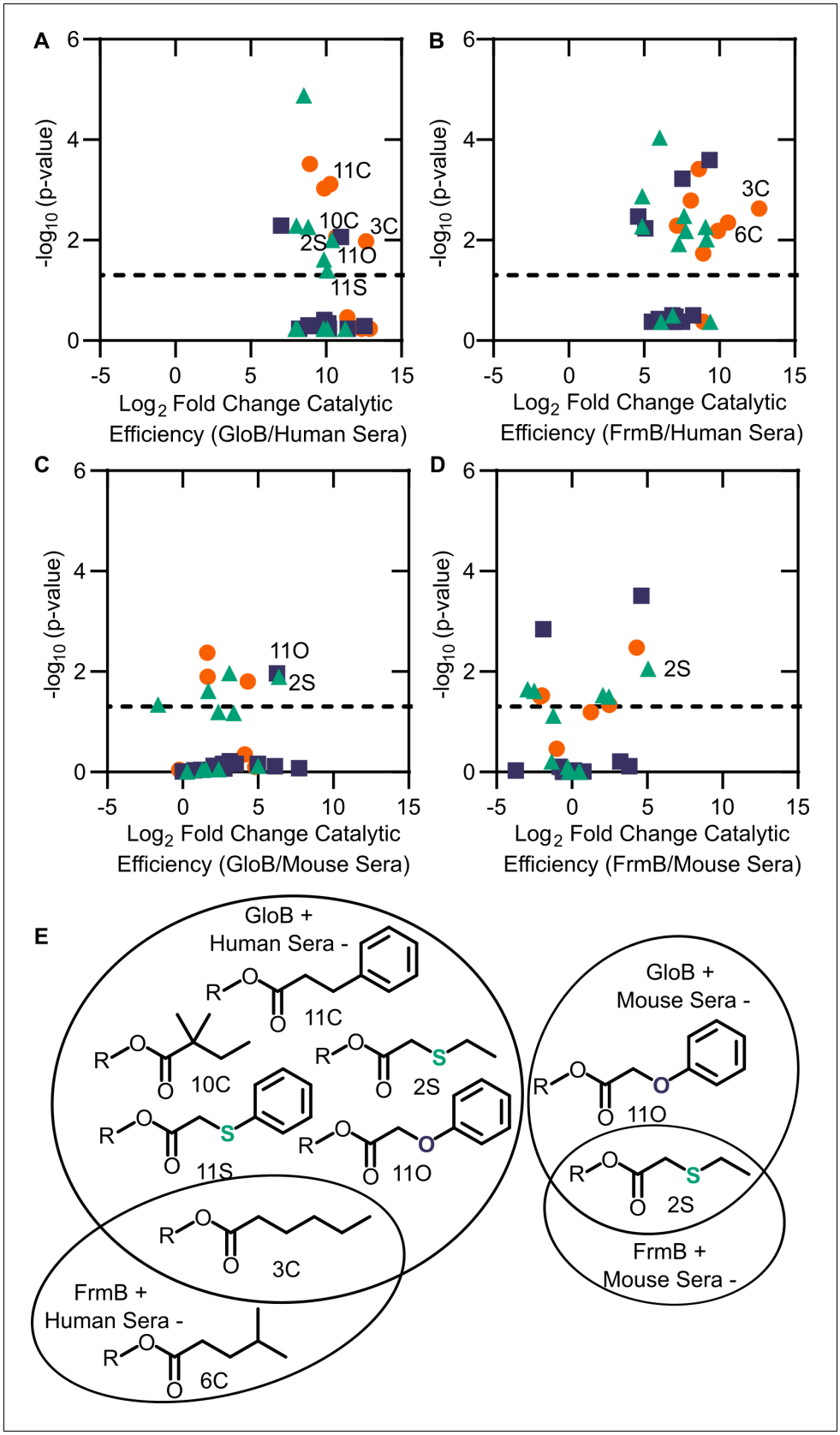

Figure 6. Comparison between microbial esterase and serum esterase catalytic efficiency. (**A–D**) Volcano plots of catalytic efficiency. Displayed are the means of three independent experiments. p-values calculated as pairwise t-

Figure 6 continued on next page

Figure 6 continued

tests with Holm-Sidak correction for multiple comparisons. (**A**) Comparison between human sera and GloB, (**B**) human sera and FrmB, (**C**) mouse sera and GloB, and (**D**) mouse sera and FrmB. (**E**) Structures of ester substrates with 210 enrichment in catalytic efficiency for microbial esterases over human serum (left) or 25 enrichment over mouse serum. Dashed line indicates a p-value of 0.05.

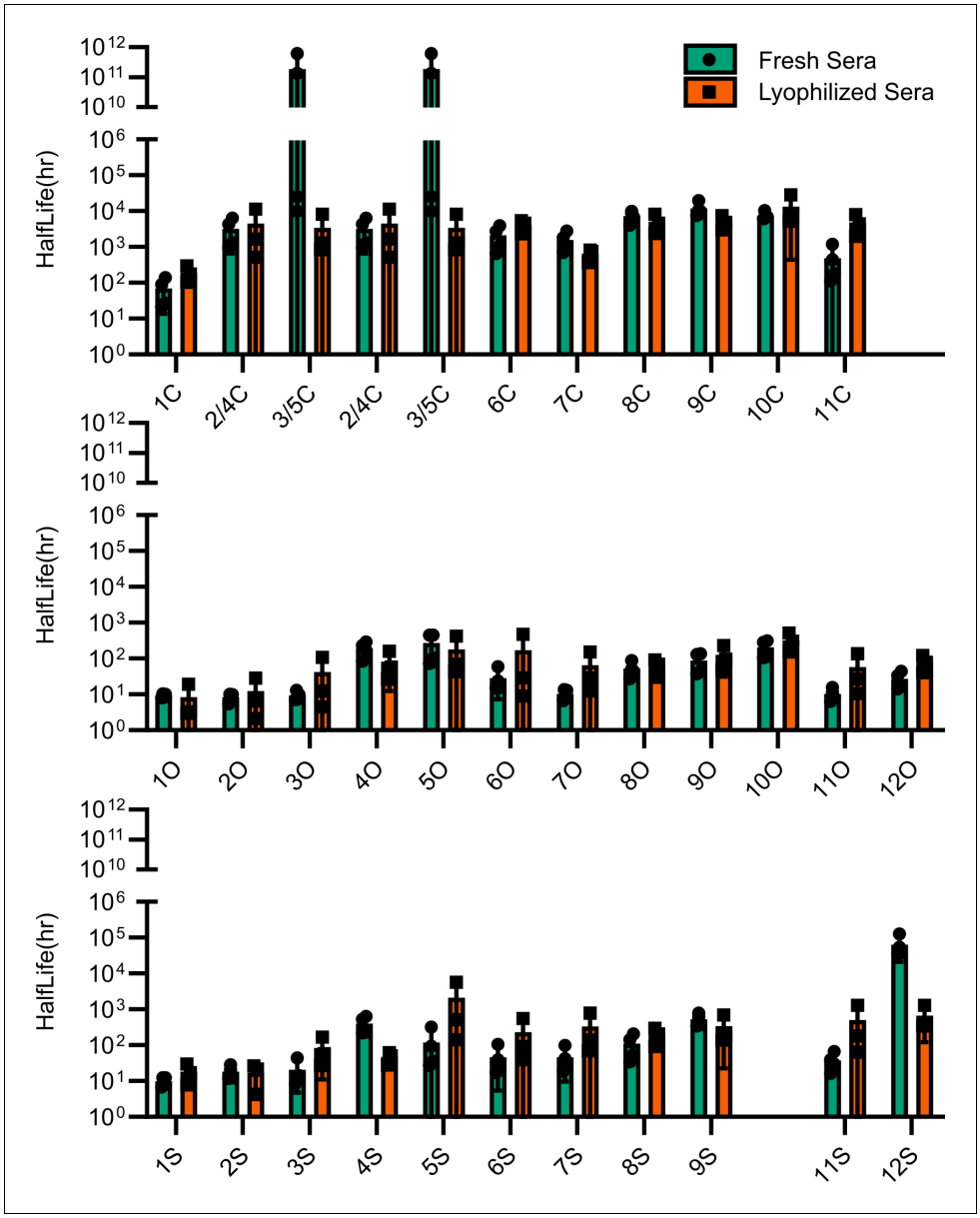

Figure 6—figure supplement 1. Comparison of esterase activity between fresh and lyophilized human sera. Points represent individual experiments; bars represent the mean ± SD of the four replicates.

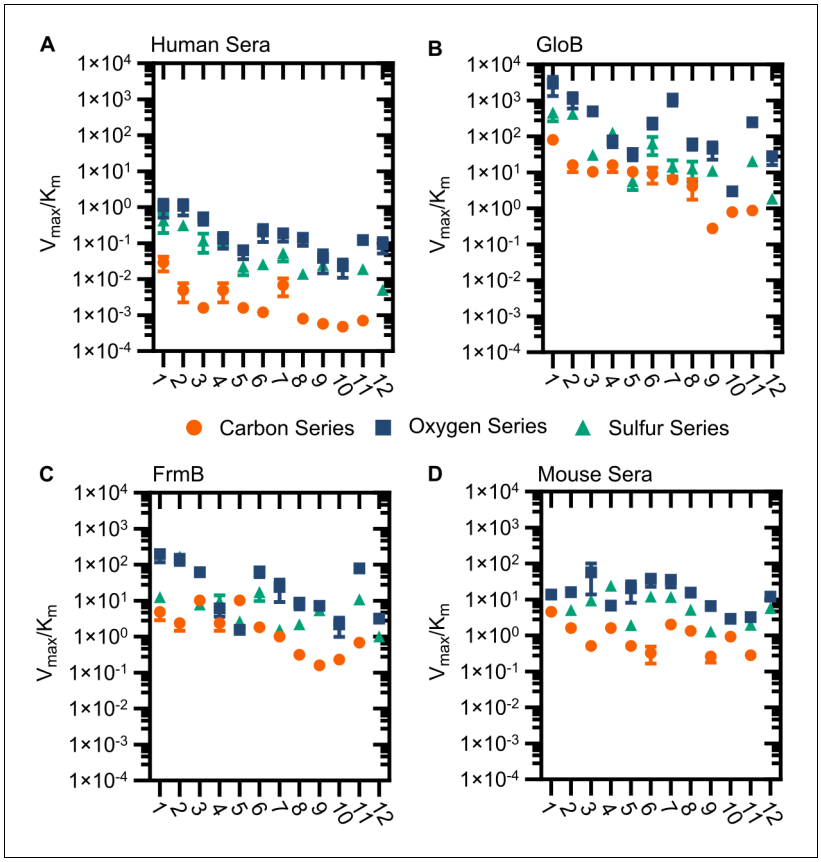

Figure 6—figure supplement 2. Modified catalytic efficiency (pmol fluorescein produced * min^{-1}*μg^{-1} protein) of (**A**) human sera, (**B**) GloB, (**C**) FrmB, and (**D**) mouse sera. X-axis corresponds to compound identities in Figure S5. Carbon containing compounds indicated in orange, oxygen in blue, and sulfur in green. Displayed are the means ± SD of three independent biological experiments.

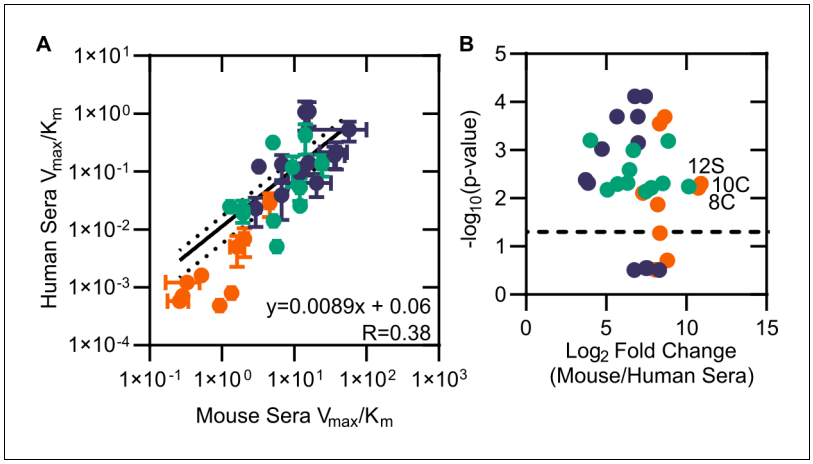

Figure 6—figure supplement 3. Comparison of mouse and human sera. (**A**) Modified catalytic efficiency (pmol fluorescein produced * min-1*µg-1 protein) of human and mouse sera. Displayed is a linear regression of the fit between mouse and human sera. (**B**) Volcano plot of catalytic efficiency. Displayed are the means of three independent experiments. p-values calculated as pairwise t-tests with Holm–Sidak correction for multiple comparisons. Dashed line indicates a p-value of 0.05.

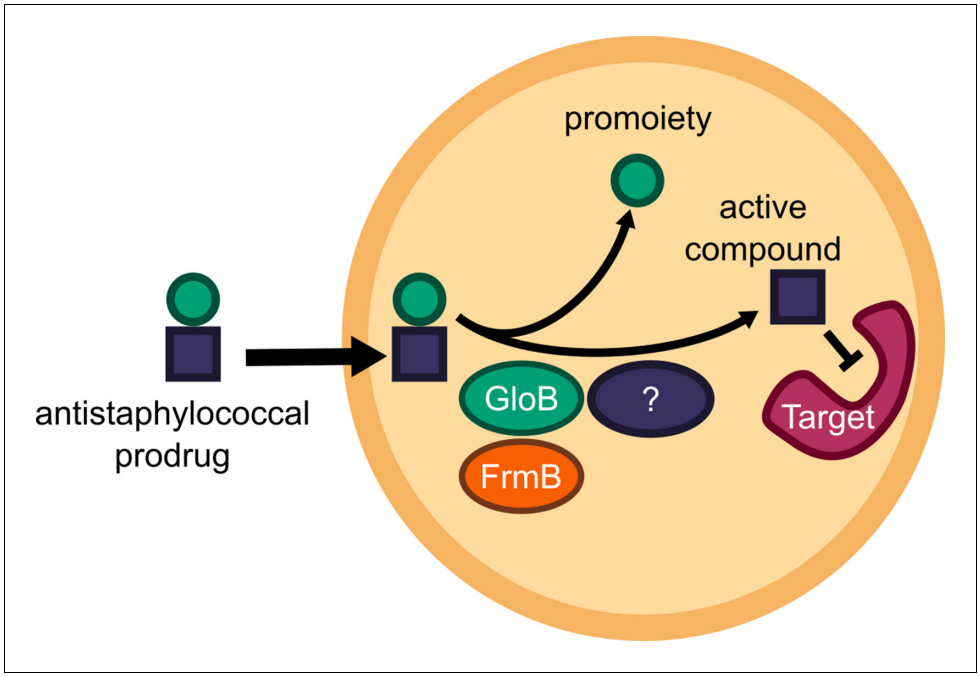

Figure 7. Model of antistaphylococcal prodrug activation. Lipophilic carboxy ester prodrugs transit the cell membrane, are first activated by either GloB or FrmB and at least one additional enzyme, before inhibiting the cellular target.